Original Paper

Effect of temperature on mineral evolution and adsorption of Eu^{3+} by bentonite in hyperalkaline conditions

Rao-ping Liao[1] , Yong-gui Chen[1,2] , Chuang Yu[3], Wei-min Ye[1,2], Dong-bei Wu[4], Cong Liu[1] and Qiong Wang[1]

[1]Department of Geotechnical Engineering, College of Civil Engineering, Tongji University, Shanghai 200092, China; [2]State Key Laboratory of Disaster Reduction in Civil Engineering, Tongji University, Shanghai 200092, China; [3]College of Environmental Protection, Zhejiang Industry and Trade Vocational College, Wenzhou 325002, China and [4]School of Chemical Science and Engineering, Tongji University, Shanghai 200092, China

Abstract

Compacted bentonite, used as an engineering barrier for permanent containment of high-level radioactive waste, is susceptible to mineral evolution resulting in compromise of the expected barrier performance due to alkaline–thermal chemical interaction in the near-field. To elucidate the mineral-evolution mechanisms within bentonite and the transformation of the nuclide adsorption properties during that period, experimental evolution of bentonite was conducted in a NaOH solution with a pH of 14 at temperatures ranging from 60 to 120°C. The results showed that temperature significantly affects the stability of minerals in bentonite under alkali conditions. The dissolution rate of fine-grained cristobalite in bentonite exceeds that of smectite, with the phase-transition products of smectite being temperature-dependent. As the temperature rises, smectite experiences a three-stage transformation: initially, at 60°C, the lattice structure thins due to the collapse of the octahedral sheets; at 80°C, the lattice disintegrates and reorganizes into a loose framework akin to albite; and by 100°C, it further reorganizes into a denser framework resembling analcime. The adsorption properties of bentonite exhibit a peak inflection point at 80°C, where the dissolution of the smectite lattice eliminates interlayer pores and exposes numerous polar or negatively charged sites which results in a decrease in specific surface area and an increase in cation exchange capacity and adsorption capacity of Eu^{3+}. This research provides insights into the intricate evolution of bentonite minerals and the associated changes in radionuclide adsorption capacity, contributing to a better understanding of the stability of bentonite barriers and the effective long-term containment of nuclear waste.

Keywords: Alkali-thermal; Alteration; Montmorillonite; Repository; Sorption; Transformation

Introduction

High-level radioactive waste (HLW), a byproduct of spent nuclear fuel reprocessing in the nuclear power industry, is distinguished by its high concentration, toxicity, heat generation, radioactivity, and long half-life (Kurniawan et al., 2022). Burying these HLWs in deep geological repositories located 400–1000 m beneath the surface has become a widely accepted permanent solution (Wang et al., 2018). These repositories typically consist of a multibarrier system, composed of a natural geological barrier and an engineered barrier system. Compacted bentonite has been chosen as the most suitable buffer material for constructing the engineered barrier due to its excellent buffering properties, including swelling and sealing properties, low permeability, and high adsorption capacity for radiotoxic waste components. On the other hand, a substantial quantity of cement or concrete materials is typically utilized in the construction of

repositories (Sun et al., 2022; Tyupina et al., 2023). However, compelling evidence indicates that the saturation of cementitious materials with groundwater decays to produce a hyperalkaline pore fluid with a pH value of up to 10~13.5 (Zhu et al., 2023). Such alkaline pore fluid has the potential to infiltrate the bentonite barrier, significantly altering its pore fluid pH, composition, and physi-chemical properties (González-Santamaría et al., 2021; Xu et al., 2011). Of particular concern is that the continuous heat emitted from the HLW decay may elevate the operating temperature of the repository to as high as 100°C (Fernández & Villar, 2010; Gens et al., 2020; Samper et al., 2020), which may speed up the dissolution rate and mineralogical changes of the active minerals within bentonite and weaken the adsorption capacity of bentonite to nuclides, presenting a significant risk to the safe operation of the repository.

Although the alkaline-thermal degradation of compacted bentonite has attracted the attention of many researchers, previous studies focus primarily on the swelling pressure (Chen et al., 2019; Karnland et al., 2007; Liu et al., 2018, 2022) and hydraulic performance (Anh et al., 2017; Ye et al., 2014). The adsorption capacity, one of the main properties responsible for preventing nuclide migration, has largely been ignored. Smectite,

as an active mineral component of bentonite, exhibits the greatest swelling performance among clay minerals. Dissolution or mineralogical alteration of smectite inevitably leads to a decay in the swelling performance of bentonite, while the implications for its adsorption properties remain ambiguous. In addition, the mineral-reaction mechanism, especially regarding secondary phases of bentonite, appears to be inconsistent across different studies, even though it is generally recognized that the degradation mechanism involves the dissolution of the active mineral smectite and the subsequent precipitation of non-expansive secondary phases (Liu et al., 2023; Zhu et al., 2023; Yokoyama et al., 2021a). As reported in the cement-bentonite or hyperalkaline-bentonite system, calcite, dolomite, jadeite, C(A)SH with variable Ca/Si ratios, potassium feldspar, illite, phillipsite, aluminite, clinozeolite, and zeolite are all likely secondary phases (Kale et al., 2021; Sun et al., 2022; Tong et al., 2022; Yokoyama et al., 2021b).

In the present study, a hyperalkaline-thermal accelerate testing program was designed to investigate the mineral evolution and adsorption capacity of bentonite. The effect of temperature on the secondary phase of bentonite and the change in adsorption capacity were studied. X-ray diffraction (XRD), scanning electron microscopy (SEM), cation exchange capacity (CEC), and N_2 adsorption-desorption were used to test the changes in mineral composition, micro-morphology, specific surface area (SSA), and pore structure of bentonite during mineral evolution. The primary objective was to reveal the mechanisms of mineral evolution of bentonite under alkaline-thermal conditions, especially the change law of the adsorption properties of nuclides, thereby providing theoretical insights to guide the design of operating temperatures for HLW deep geological repositories and to evaluate the evolution of bentonite's long-term buffering properties.

Experimental

Materials and reagents

Sodium bentonite has been selected by many countries as a buffer/backfill material for high-level waste disposal warehouses because of its greater swelling performance than calcium bentonite; typical such bentonites include MX-80 sodium bentonite in Wyoming, FEBEX sodium bentonite in France, Kunigel V1 sodium bentonite in Japan, and GMZ sodium bentonite in China (Ye et al., 2010). Considering that the sodium ion is also the main cation in the groundwater of most repositories, especially in some offshore sites, purified sodium bentonite without complex mineral components was selected as the experimental soil. The purified sodium bentonite was purchased from Shanghai Darui Fine Chemicals Co., Ltd (Shanghai, China) for the experiments; it contained smectite (65.3%) and a small amount of cristobalite (34.7%) according the XRD results shown below. Before use, the raw bentonite was subjected to drying in an oven at 105°C for 48 h and crushing to a particle size of <15 um (passing through an 800-mesh sieve), then stored in a desiccator. The sodium bentonite had a CEC value of 82.51 cmol/kg. Eu^{3+}, which is safe and readily available, non-radioactive, and has a similar ionic radius to the nuclide ion, is generally considered an acceptable nuclide and is used in many laboratories (Kyzioł-Komosińska et al., 2019; Liao et al., 2023; Wang et al., 2015). Therefore the Eu^{3+} was selected as the adsorbate by dissolved europium nitrate ($Eu(NO_3)_3 \cdot 6H_2O$) in this experiment. All chemicals used in the experiment were purchased from Shanghai Aladdin Biochemical Technology Co., Ltd.

(Shanghai, China) and were >99.5% pure. Deionized water was used to prepare all solutions for the experiment.

Methods and characterizations analysis

Mineral evolution test

The mineral evolution of bentonite in an alkaline environment was examined in a sodium hydroxide (NaOH) solution with a pH of 14 to ensure that only Na^+ cations were present in the system. Specifically, a total of 20 g of bentonite was dispersed in 250 mL of NaOH solution and sealed within a 300 mL hydrothermal reaction vessel, which was then heated in a constant-temperature oven. The experimental temperature range was set from 60 to 120°C, partitioned into four distinct stages: 60°C, 80°C, 100°C, and 120°C. A sequential progression through these temperature stages was used, with the sample undergoing a reaction phase at 60°C for a period of 15 days (excluding a 12 h cooling period), and then continuing to the next stage (Ramírez et al., 2002; Rozalen et al., 2009). The dissolved bentonite at each stage was obtained by taking out the corresponding evenly divided, dispersed slurry, then washing it repeatedly to remove excess alkali and soluble phases with deionized water using a high-speed centrifuge at 8000 rpm for 10 min (equivalent to 5867×*g*; XiangYi-H1850, Changsha, China), and finally mashing and passing it through a 200-mesh sieve after oven-drying at 105°C. Subsequently, batch adsorption and a series of characterization tests were carried out with these dissolved bentonite samples. Under alkaline-thermal conditions, bentonite must undergo mineral dissolution and transformation. As a result, bentonite samples obtained after various stages of reaction were referred to as 'dissolved bentonite'.

Batch-adsorption experiments

Eu^{3+} was employed as the adsorbate to investigate the variation in adsorption capacity as it is a chemically homogeneous trivalent lanthanide with no radiation effects at the molecular level. Detailed operations are as follows: a fixed amount of 0.1 g of dissolved bentonite was used as the adsorbent and added to a 15 mL resin centrifuge tube containing 10 mL of Eu^{3+} solution; the mixture was then shaken in a thermostatic water bath oscillator at room temperature for 12 h; subsequently, the solution was separated from the solids by centrifugation using a XiangYi-H1850 instrument (Xiangyi, Changsha, China) at 8000 rpm (~5867×*g*) for 3 min (excluding the acceleration phase) and filtered using a 0.45 um membrane filter; finally, the residual Eu^{3+} in the aqueous solution was measured using a Flame Atomic Absorption Spectrophotometer (Shimadzu AA6880F, Kyoto, Japan) with a C_2H_2-N_2O flame; adsorption wavelengths were 459.4 nm, without any background interference. The amount of Eu^{3+} adsorbed was calculated based on the difference in the concentrations before and after adsorption in the aqueous solution. All experiments were conducted in duplicate. The pH of the Eu^{3+} solution was adjusted to 7.9 by adding 0.01 M HCl or NaOH solutions, considering the groundwater environment of the Beishan Geological Repository of China (Wang et al., 2018). Although Eu^{3+} exists in different hydrolyzed forms in this pH solution, the adsorption capacity of bentonite for it changes very little because Eu^{3+} in the adsorbed state does not participate in constructing the equilibrium of the hydrolysis reaction according to the previous results (Liao et al., 2023). Considering that the factors influencing bentonite's adsorption of Eu^{3+} have been fully explored in previous work by the present authors, only the isothermal adsorption curves of bentonite were tested in the present study.

Characterization

Analysis by XRD was conducted using a Bruker D8 Advance X-ray diffractometer (Bruker, Karlsruhe, Germany), operated at 40 kV and 40 mA, with CuKα (λ = 1.5406 Å) irradiation, and a scanning rate of 0.15 s/step in the 2θ range of ~3–65°. The microstructure of the dissolved bentonite samples was examined using scanning electron microscopy with an FEI Nova NanoSEM 200 instrument (Hillsboro, Oregon, USA). The SEM images were taken at magnifications ranging from ×20 to ×80,000, with a secondary electron imaging resolution of 1 nm at 15 kV. The SSA and pore distribution were measured by physical adsorption of N_2 at 77 K using an ASAP2020HD88 automatic physical adsorption instrument provided by Micromeritics Instrument Corporation (Norcross, Georgia, USA), and analyzed by the Brunauer–Emmett–Teller (BET) and Langmuir methods within the fitting interval for P/P_0 which ranged from ~0.05 to 0.2. The CEC of bentonite samples was measured according to the bentonite standard of China (GB/T 20973-2020) using $BaCl_2$ and $MgSO_4$ as the exchanger. The CEC value was calculated by detecting the reduction of Mg^{2+} after replacement because the interlayer Ba^{2+} had been completely precipitated by SO_4^{2-}.

Theoretical approach

The adsorption capacity (Q_e, cmol/kg) of Eu^{3+} was calculated using Eqn 1:

$$Q_e = \frac{(C_i - C_e)}{m_{ads}} V \quad (1)$$

where C_i and C_e are the initial and equilibrium concentrations of the Eu^{3+} solution (mM), respectively, V is the volume of Eu^{3+} solution (mL), and m_{ads} is the mass of the bentonite (kg).

The equilibrium experimental data for the adsorption of Eu^{3+} on the composite was analyzed using the Langmuir and Freundlich isotherm models (Langmuir, 1918) applied to describe the adsorption data. The Langmuir model is represented in Eqn 2:

$$Q_e = \frac{Q_m b C_e}{1 + b C_e} \quad (2)$$

It can be expressed in linear form as:

$$\frac{C_e}{Q_e} = \frac{1}{b Q_m} + \frac{C_e}{Q_m} \quad (3)$$

where Q_e (cmol/kg) related to the adsorption capacity is the maximum amount of adsorbent at the complete monolayer coverage, and b is the Langmuir equilibrium constant, which is related to the heat of adsorption.

The Freundlich expression (Freundlich, 1907), an empirical relation describing adsorption to heterogeneous surface is given by:

$$Q_e = K_F C_e^n \quad (4)$$

and, analogously, the linear form is expressed as:

$$\log Q_e = \log K_F + n \log C_e \quad (5)$$

where, K_F and n are the Freundlich coefficients; the former represents the adsorption capacity when the metal ion equilibrium concentration equals to 1, and the latter represents the degree of dependence of the adsorption on the equilibrium concentration.

Results

Mineral evolution under alkaline conditions

Effect of temperature on mineral compositions

The main constituents of the raw bentonite used are smectite ($Na_x(Al,Mg)_2(Al,Si)_4O_{10}(OH)_2 \cdot nH_2O$) and cristobalite; no other clay minerals were detected by XRD (Fig. 1). The basal reflection (001 or d_{001} value) of smectite at 6.28°2θ was measured by XRD
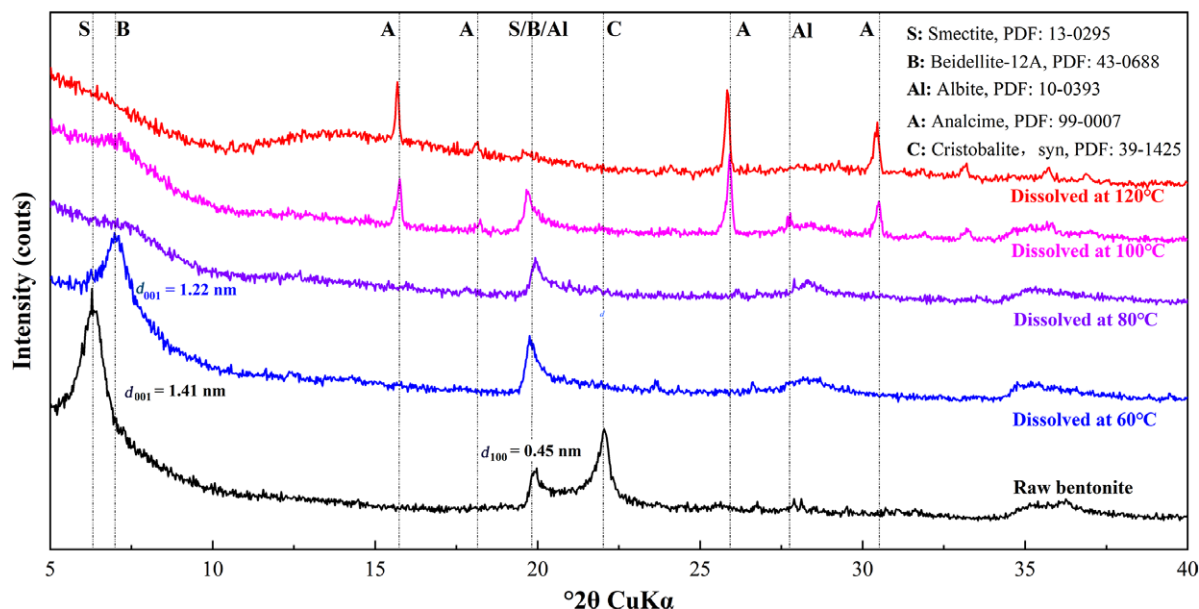

Figure 1. Mineral evolution analysis of dissolved bentonite samples.

from the two surfaces of smectite crystal layers. Specifically, after 15 days of exposure to NaOH solution (pH=14) at a temperature of 60°C, the cristobalite in the bentonite disappeared completely, and the distance between the smectite crystal layers decreased. When the temperature was increased to 80°C, the basal reflection of the smectite was no longer detected, and a new aluminum silicate mineral, albite ($NaAlSi_3O_8$), appeared in the system, according the common reflection with smectite at 19.8°2θ and the unique characteristic signal at 27.7°2θ. As the sample continued to be exposed to the hyperalkaline environment at 100°C, another new mineral, analcime ($NaAlSi_2O_6 \cdot H_2O$), was found. With the temperature further increasing to 120°C, the characteristic reflections of albites in the clay samples disappeared completely, leaving only those representing analcime. The test results show the evolution process of smectite transforming into albite, and then into analcime.

Effect of temperature on SSA and pore distribution

The adsorption and desorption curves of dissolved bentonite powders on N_2 illustrate effectively the SSA and pore characteristics, as demonstrated in Fig. 2 and Table 1. The adsorption of N_2 by bentonite underwent three stages: monolayer adsorption, multilayer adsorption, and capillary condensation. The desorption regression adsorption curve in Fig. 2a exhibits morphological characteristics that correspond to a type-II adsorption curve, as defined by the adsorption type classification specified by the International Union of Pure and Applied Chemistry (IUPAC) (Al-Ghouti and Da'ana, 2020; Wang and Guo, 2020). The rapid regression at the end of desorption and the convergence of the adsorption curve were the typical features of slit pores, which align perfectly with the layered structure of bentonite. Furthermore, the hysteresis loop of adsorption-desorption narrows rapidly and even exhibits an open mouth shape, which indicates that the

Table 1. Fitting results of N_2 monolayer adsorption capacity and surface area of samples

Bentonite samples	BET method				Langmuir method			
	V_m (cm³/g)	S_{BET} (m²/g)	C	R^2	V_m (cm³/g)	S_{Lang} (m²/g)	b	R^2
Raw bentonite	11.63	50.62	90.55	0.9999	14.83	64.56	38.56	0.9988
Dissolved at 60°C	1.80	7.85	323.60	0.9998	2.25	9.79	65.07	0.9999
Dissolved at 80°C	0.61	2.67	102.29	0.9992	0.76	3.29	49.59	0.9950
Dissolved at 100°C	0.52	2.27	23.11	0.9996	0.71	3.07	14.57	0.9865
Dissolved at 120°C	2.30	10.00	52.20	0.9999	3.01	13.12	26.51	0.9999

Note: V_m is the adsorption capacity of N_2 when the surface of soil particles is covered by a single layer; S_{BET} is the specific surface area calculated by the BET method; C is the coefficient of the BET model. S_{Lang} is the specific surface area calculated by the Langmuir method; b is Langmuir model coefficient; R^2 is the correlation coefficient of linear fitting of the corresponding model.
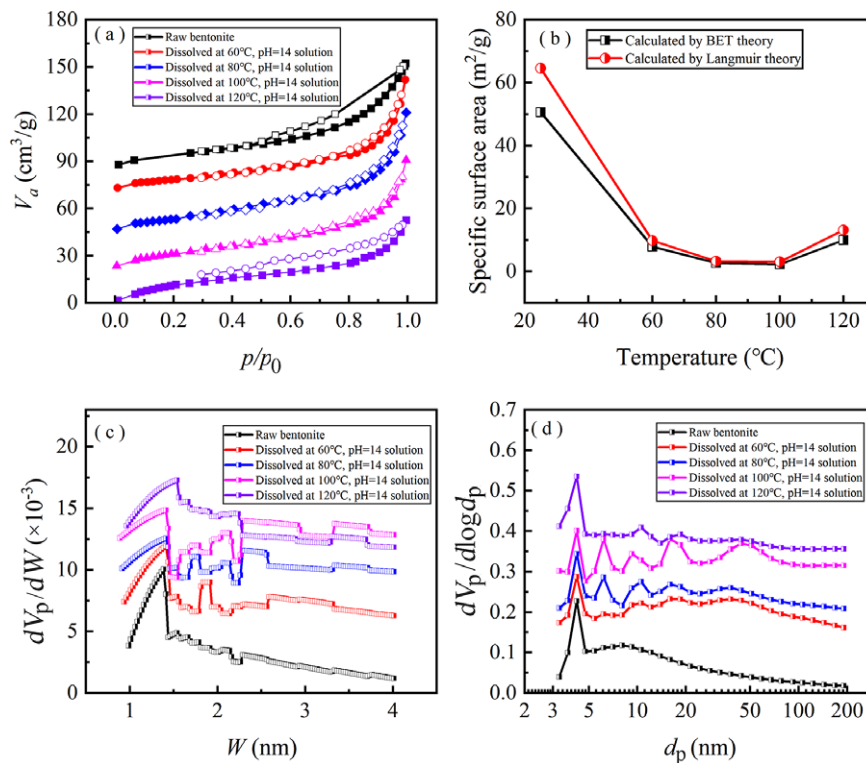

Figure 2. Results of BET-N_2 absorption and desorption of dissolved bentonites: (a) N_2 adsorption-desorption curve; (b) change of SSA with temperature; (c) pore distribution from the Horvath-Kawazoe (HK) method; (d) pore distribution from the Barrett-Joyner-Halenda (BJH) method.

pore morphology changes to ink-bottle type. The decrease in N_2 adsorption also reflects the fact that the SSA of bentonite decreases rapidly due to the reaction with alkali (Fig. 2b), even at the initial stage of 60°C when the structure of smectite seems to undergo no significant change according to XRD results.

The characteristic pore sizes of the sample were reflected by the peak positions. The BJH mesopore distribution demonstrates that the typical mesopore size of raw bentonite was only 4.5 nm. However, after a certain amount of reaction, the pore size increases, and new characteristic pores emerge, such as those at 6, 10, 18, and 50 nm (Fig. 2c). Mesopore is usually the size of the
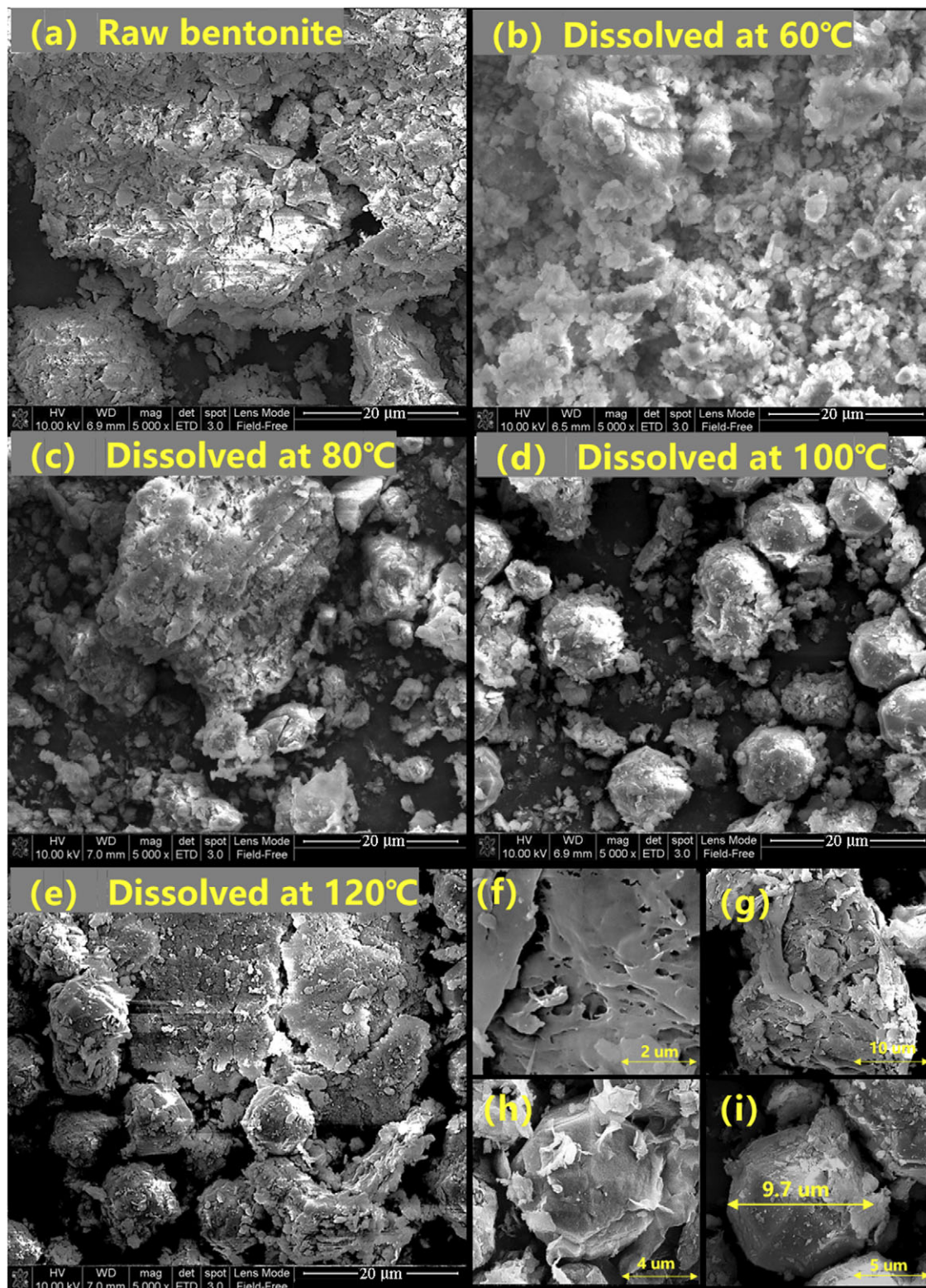

Figure 3. Characteristic images of the evolution of bentonite in alkaline-thermal environments.

pore between mineral assemblages, and the formation of new pore characteristics corresponds to the production of new minerals. The increase in mesoporous pore size indicates that during the process of alkaline-thermal dissolution, the aggregates of smectite which should have undergone swelling and cracking gradually coalesce to form mineral particles, and the particle size increases with the dissolution of smectite. The Horvath Kawazoe (HK) micropores are examples of the stacked pores of the mineral crystal cells (Fig. 2d). The peak concentration of raw bentonite at 1.41 nm corresponds to the interlayer spacing of smectite. At 60°C, the change in bentonite was minimal. However, new micropore features occurred at 80 and 100°C along with the rapid dissolution of smectite and the generation of new minerals. A stable, concentrated distribution was finally formed due to the completion of mineral evolution at 120°C.

Effect of temperature on microstructure

The microstructure changes of the dissolved bentonites were observed by SEM (Fig. 3) illustrating that the micro-morphology of raw bentonites (mainly smectite) was a tightly stacked layered structure (Fig. 3a); however, following alkaline-thermal dissolution at 60°C, the layered smectite layers became very broken and feature sharp edges (Fig. 3b); subsequently, the broken smectite layers began to coalesce after dissolution at 80°C; upon heating at 100°C, the soil sample in the field of view had basically turned into small spherical (regular polyhedral) analcimes, an isometric zeolite mineral with a tetrakisoctahedron mineral aggregate, as shown in Fig. 3d; similarly, at 120°C, a large number of analcime particles can also be seen in the field of view, which also indicates that analcime is the most stable mineral at this temperature. In addition, dissolved bentonite was found to have dissolved (or eroded) cavities (Fig. 3f) or elongated split sheets (Fig. 3g), which were absent in unreacted bentonite. These phenomena suggest that dissolution began both in the middle of the surface of smectite crystals and developed gradually through reaction splitting at the edges. The complete evolution process of bentonite under an alkaline-thermal environment can be divided into three stages (depicted in Figs 3f–i): initially, certain active sites on the base layer and edges of the smectite were dissolved preferentially, resulting in the formation of cavities and split sheets; subsequently, the smectite layers broke into fragments with sharp edges; ultimately, the fragments evolved into particles of analcime.
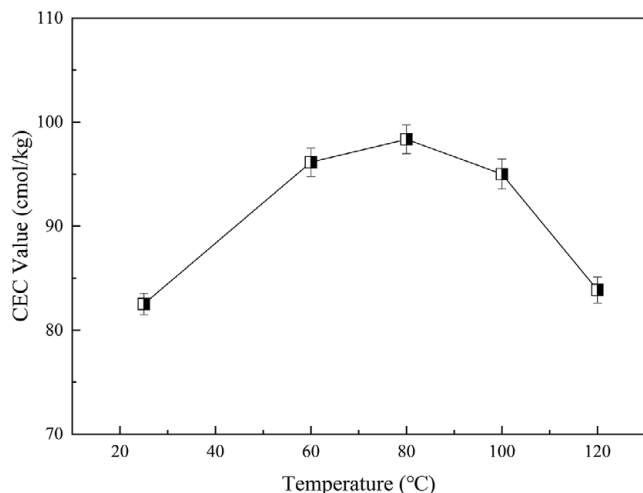

Figure 4. CEC evolution for bentonite in an alkaline-thermal environment.

Adsorption evolution under alkaline conditions

Effect of temperature on CEC

Surface complexation and ion exchange are two fundamental mechanisms responsible for ion adsorption on clay surfaces. In the case of bentonite, ion exchange is the primary mode of adsorption. The CEC is a crucial characteristic of bentonite that exhibits a positive correlation with its swelling behavior and adsorption capacity. The CEC of bentonite increased and subsequently decreased as the ambient temperature rose (Fig. 4). The CEC value of the raw bentonite was 82.51 cmol/kg; after the alkaline-thermal reaction, the dissolved bentonite reached a maximum of 98.35 cmol/kg at 80°C, and decreased to 83.86 cmol/kg at the final temperature of 120°C.

Effect of temperature on adsorption of Eu^{3+}

The isothermal adsorption curve is a critical indicator for describing the adsorption behavior of materials. The isothermal adsorption process of Eu^{3+} on bentonite demonstrates a rapid increase in adsorption capacity with equilibrium concentration at low concentrations, followed by stabilization (Fig. 5). The type of curve in Fig. 5a conforms to the type-I(b) isotherm classification according to the according to the standards set by IUPAC (Al-Ghouti and Da'ana, 2020; Wang and Guo, 2020. The Langmuir and Freundlich models were employed to analyze the isothermal adsorption results of the aforementioned soil samples, and the corresponding outcomes are displayed in Figs 5b, and 5c, respectively. In comparison to the Freundlich model, the Langmuir model exhibits significantly better fitting performance for bentonite at all dissolution stages. Consequently, the Langmuir fitting results were utilized as a reference for determining the maximum adsorption capacity of bentonite for Eu^{3+} at each dissolution stage (Fig. 5d).

Similar to the trend observed in CEC, the maximum adsorption capacity of bentonite samples for Eu^{3+} also follows a pattern of initial increase and subsequent decrease with rising temperatures in the alkaline environment. The maximum adsorption capacity of Eu^{3+} for raw bentonites was 26.18 cmol/kg initially; then, the dissolved bentonite reached a peak value of 85.47 cmol/kg at 80°C before decreasing to 31.35 cmol/kg at the final temperature of 120°C.

Discussion

Phenomenon analysis of changes in microscopic characteristics

The dissolution sequence and secondary phases of minerals in bentonite are controversial. Although some reports have speculated on the proportion of Si/Al elements dissolved in cristobalite over smectite through the initial chemical reaction of bentonite and alkali solution (Karnland et al., 2007; Cuevas et al., 2022), definitive proof has been absent from the discourse. However, the present experiment, bolstered by XRD analysis, now offers direct evidence that clarifies these dissolution sequences. Some alkaline alteration tests of compacted bentonite with little change in cristobalite content may be caused by the stability of the equilibrium of cristobalite dissolution due to the slow migration of silica tetrahedral groups dissolved in pore solution, in addition to the fact that it is difficult to observe accurately the slight reduction of cristobalite (Fernández and Villar, 2010; Tong et al., 2022; Zhang et al., 2020). As for the phase transition of smectite in mineralogy, reduction in the interlayer spacing in smectites after alkaline-thermal reaction

(or corrosion) has been reported widely (Karnland et al., 2007; Tong et al., 2022). Discussion about the transformed secondary phases of minerals after dissolution is not consistent, however, and it is thought that this is certainly related to the ionic composition of the system. Illite, orthoclase, albite, and clinoptilolite were detected by Tong et al. (2022) in the compacted GMZ-Na bentonite soaked in KOH solution. Feldspar and zeolite were detected by Cheshire et al. (2014) in K-Ca-Na-Cl solution (~1900 mg/L total dissolved solids) in a heated environment of Wyoming bentonite, and the latter authors found that the combination of a Na-rich environment, limited K supply, and precipitation of Al-bearing minerals (analcime and feldspars) appears to have inhibited the formation of illite-smectite mixed layers. A clearer explanation for this controversy is that the phase transition of smectite occurs sequentially, first converted to albite, and then to analcime in the Na-rich environments in this experiment.

The evolution stages of bentonite at various temperatures were revealed by SEM (Fig. 3f–i). This phenomenon aligns with XRD results, and is consistent with results reported by Cheshire et al. (2014), Tong et al. (2022), and Zhang et al. (2020). An interesting point from previous studies which merits discussion involves speculation that the alkali dissolution of smectite occurs preferentially at the active hydroxyl (=Si/Al-OH) site on the edge of the crystal due to deprotonation hydrolysis. The question remains,

however, whether the tetrahedral surface contains unstable active sites. The corrosion phenomena of cavity (Fig. 3f) and split (Fig. 3g) seem to indicate the presence of unstable active sites (Si-O-Al) on the basal surface of the tetrahedral sheet, which may be caused by the substitution of lattice atoms (see the red circle in Fig. 6). The observation by Grybos et al. (2010) also supports this viewpoint that the dissolution of Fe(III) in smectite crystals did not correlate with an increase in the surface area of the smectite edge or a decrease in grain size. Some have argued that smectite dissolution proceeded via edge dissolution, as atomic force microscopy (AFM) does not observe any corrosion pits on the basal surface. Of course, the AFM could have missed it because the area of the crystal being tested is too small. The dissolution and secondary phases of minerals in the SEM view can explain the evolution results of SSA and pore space in the adsorption data of N_2. Specifically, the initial consolidation of smectite layers led to a rapid decrease in SSA; the formation of new minerals resulted in the evolution of new micropores; and the columnar pores of analcime were also the main reason why the N_2 adsorption and desorption curve cannot be closed.

Speculation on the evolutionary mechanism of smectite

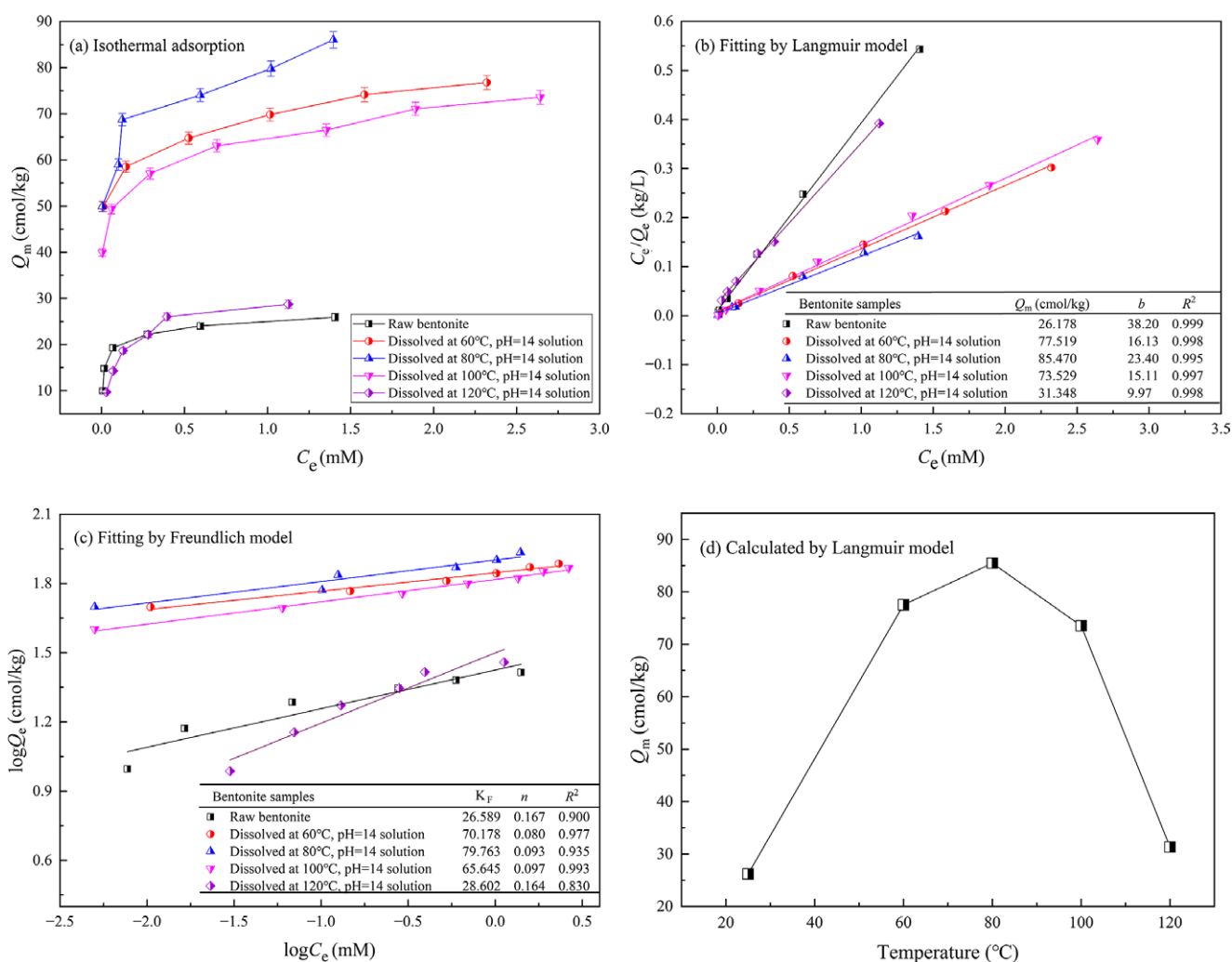The crystal structure of smectite comprises two tetrahedral silica sheets (SiO_4) and an octahedral Al-O ($Al(O, OH)_6$) sheet

Figure 5. Characteristics of the evolution of adsorption of Eu^{3+} by bentonite in alkaline-thermal environments.

sandwiched in between. This arrangement forms a 2:1 structure and belongs to the 'monoclinic' crystal system. Frequently, the Si(IV) in the SiO_4 tetrahedron is replaced by Al(III) (up to 15%), while the Al(III) in the $Al(O, OH)_6$ octahedron can be replaced by lower-valence cations such as Mg(II). This substitution results in an excess (or permanent) negative charge of 0.2–0.6 per cell (García-Romero et al., 2021). To balance the crystal layer charge of smectite, a large number of exchangeable metal cations (e.g. Na^+, Ca^{2+}, Mg^{2+}, K^+, etc.) and water molecules are adsorbed between the layers. Accordingly, the smectite has significant swelling, poor permeability, and strong adsorption. Generally, the theoretical chemical formula of smectite can be expressed as $(M_x \bullet nH_2O)$ $(Al_{2-y}Mg_y)[(Al_zSi_{4-z}O_{10})](OH)_2$, where M stands for the adsorbed cations, x is the number of adsorbed cations and y and z are the unknown numbers of substitutions. For the bentonite used in the present experiment, the interlayer exchangeable ions of montmorillonite minerals were mainly Na^+.

The series of phenomena observed in this experiment indicate that smectites dissolve and transform into different steady-state structure minerals in alkaline environments at varying temperatures. The evolution of minerals essentially involves the process of partial chemical bond breaking and recombination. Lamellar silica-aluminate minerals are significantly less stable than framework structures. Longer bond lengths correspond to smaller bond energies and increased susceptibility to breakage. The $(Si/Al)O_4$ tetrahedron is the fundamental and stable basic

structure of minerals. When considering the lengths of chemical bonds of minerals during the evolution of bentonite in Table 2 (Refson et al., 2003; Wang et al., 2011), the $O–O_{(oct)}$ bond, connecting a silico-oxygen tetrahedron to an aluminum-oxygen octahedron, is clearly the longest in the smectite mineral. The commonly accepted reaction mechanism posits that the smectite dissolution is catalysed by protonated Al-OH groups, on the bridging O atoms of both Al-O-Si sites (located only on the {110} surfaces), and Al_2-O-Si sites on the {010} and {110} surfaces (Kuwahara, 2006). For the site of isomorphic substitution in the aluminum-oxygen octahedron, as the weak sites of the structure, it is also easy to break the bond and collapse it in the process of dissolution. Therefore, the dissolution process of smectite minerals includes both the shrinkage dissolution of the extended edge and the collapse and destruction of the aluminum-oxygen octahedral sheet. The dissolution rate depends mainly on the break of the bridging oxygen bond in the crystal (Rozalen et al., 2009). Based on the results obtained from the aforementioned tests and previous studies, the evolution process of smectite in an alkaline-thermal environment can be inferred as depicted in Fig. 6.

The evolution process of smectite to analcime can be divided into three stages. The first stage corresponds to the breaking of the $O–O_{(oct)}$ bond and the bridge bond of Al–O–Si in smectite at 60℃. During this stage, the primary structure of smectite is largely preserved, and the crystal layer spacing is reduced, as indicated by XRD results. However, the significant alteration in SSA and CEC

Table 2. Bond lengths of the chemical bonds in the crystal structures of minerals (Refson et al., 2003; Wang et al., 2011)

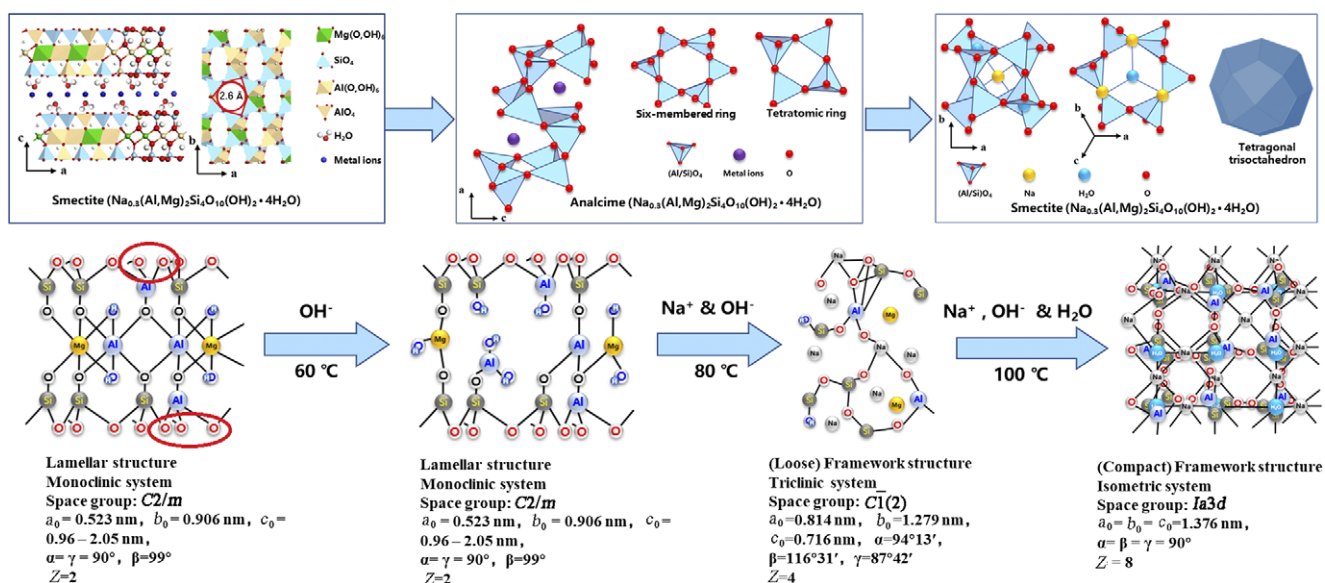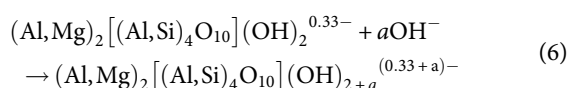| Smectite	Bond lengths (nm)	Albite	Bond lengths (nm)	Analcime	Bond lengths (nm)
O–O	0.2620 –0.2690	Si–O	0.1603–0.1656	Si/Al–O	0.1629
Si/Al–O	0.1620–0.1660	Al–O	0.1748–0.1764	Si/Al–Si/Al	0.3127
Al/Mg–O(oct)	0.1910–0.2180	Na–O	0.2448–0.2978	Si/Al–Na	0.3578
O–O(oct)	0.3028			Na–H₂O	0.2420
O–H	0.1011			Na–O	0.2498
				Na–Na	0.4192

Figure 6. Schematic diagram of mineral-structure evolution of bentonite in alkaline-thermal environments.
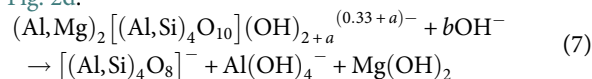
values suggest substantial changes within the structure. The increase in CEC implies a potential increase in the negative charge of the smectite unit cell (Karnland et al., 2007). The most probable scenario is that the Al/Mg(O,OH)$_6$ octahedron within the lattice breaks due to the rupture of the O–O bond, leading to a collapse to some extent and a decrease in the spacing between the crystal layers. Considering that the diameter of the hexagonal pore enclosed by a silicon-oxygen tetrahedron on the basal surface of smectite is ~2.6 Å (Sposito et al., 1999), the hydrated diameter (D_H) of metal ions (in Table 3) (Nightingale, 1959) such as $D_{H(Na^+)}$ = 7.16 Å, $D_{H(Mg^{2+})}$ = 8.56 Å, $D_{H(Al^{3+})}$ = 9.5 Å, are too large to pass through (even Stokes' diameter). Consequently, the two-layer silica tetrahedral network creates a filtering effect, blocking the cations and enabling OH$^-$ ions to enter the crystal layer, thereby maintaining or even increasing the negative charge of the lamellar structure. For the Na-smectite utilized in the present experiment, the chemical reaction process can be represented by Eqn 6:

$$(Al,Mg)_2 \left[(Al,Si)_4 O_{10} \right] (OH)_2^{0.33-} + aOH^-$$
$$\rightarrow (Al,Mg)_2 \left[(Al,Si)_4 O_{10} \right] (OH)_{2+a}^{(0.33+a)-} \quad (6)$$

where a represents an unknown number, depending on how many Al atoms are replaced by Mg atoms in the lattice.
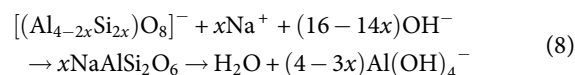
When the temperature continued to rise to 80°C, bentonite entered the second evolution stage. At this stage, the reflection peak of {001}, which belonged to the smectite crystal layer, disappeared completely. Only the {020} reflection peak of the silicon-oxygen tetrahedron (García-Romero et al., 2021), along with the basic reflection peak of albite, remain. The aluminum-oxygen octahedron within the crystal structure of smectite underwent complete disintegration. Furthermore, the planar silicon-oxygen tetrahedra were broken, and reassembled into new, loose, framework-like structure albite minerals, as shown in Eqn 7. The original tetrahedral structures, which were connected via oxygen bridges, subsequently break to generate numerous new adsorption active sites (-OH), leading to the rapid increase in CEC and adsorption capacity. The transformation of minerals is also evident from the emergence of a new micropore characteristic peak in Fig. 2d.

$$(Al,Mg)_2 \left[(Al,Si)_4 O_{10} \right] (OH)_{2+a}^{(0.33+a)-} + bOH^-$$
$$\rightarrow \left[(Al,Si)_4 O_8 \right]^- + Al(OH)_4^- + Mg(OH)_2 \quad (7)$$

where a and b represent unknown numbers, depending on how many Si and Al atoms are replaced in the lattice. Note that even in alkaline solutions, Mg atoms may not precipitate completely and free ions may also be present.

When temperatures were >100°C, a new phase of mineral evolution took place, where where albite continued to transform into more stable analcime (Liu et al., 2021). The final mineral may also be other zeolite group minerals when more calcium, magnesium, and potassium ions are present (Fernández et al., 2006; González-Santamaría et al., 2021; Lee et al., 2023; Ye et al., 2016). One certainty is that when cations are involved in the construction of new minerals, any excess negative charge must be eliminated resulting in a reduction in CEC. In addition, the limited pore size imposes significant restrictions on the adsorption and exchange of cations. The process of mineral transformation from albite to analcime is essentially a process in which tetrahedral structures are cohesive and pore sizes decrease. The reaction principle can be represented by Eqn 8.

$$\left[(Al_{4-2x}Si_{2x})O_8 \right]^- + xNa^+ + (16-14x)OH^-$$
$$\rightarrow xNaAlSi_2O_6 \rightarrow H_2O + (4-3x)Al(OH)_4^- \quad (8)$$

where x represents an unknown number, depending on how many Si atoms are replaced by Al atoms in the tetrahedral lattice.

Analysis of the evolution of adsorption capacity of bentonite

Theoretically, the adsorption capacity for Eu^{3+} by dissolved bentonite should include the adsorption capacity of the chemical complex and the physical adsorption capacity of cation exchange. Given that the CEC is determined for a single valence, a comparison between the maximum adsorption capacity and 1/3 of the CEC is illustrated in Fig. 7. The adsorption capacity of Eu^{3+} is close to 1/3 CEC when the mineral sample is uneroded smectite or analcime.

Table 3. Comparison of radii of common ions in aqueous solution (Nightingale, 1959)

Ion species	D_c (Å)	D_s (Å)	D_H (Å)
H$^+$	-	(0.56)	(4.56)
Na$^+$	1.9	3.68	7.16
K$^+$	2.66	2.5	6.62
NH$_4^+$	2.96	2.5	6.62
Mg^{2+}	1.3	6.94	8.56
Ca^{2+}	1.98	6.2	8.24
Fe^{2+}	1.5	6.88	8.56
Fe^{3+}	1.2	8.12	9.14
Al^{3+}	1	8.78	9.5
OH$^-$	3.52	(0.92)	(6.00)
Cl$^-$	3.62	2.42	6.64
NO$_3^-$	5.28	2.58	6.7
CO$_3^{2-}$	5.32	5.32	7.88
SO$_4^{2-}$	5.8	4.6	7.58

D_c is the ionic crystal radius; D_s is the ionic Stokes radius; D_H is the hydrated ion radius
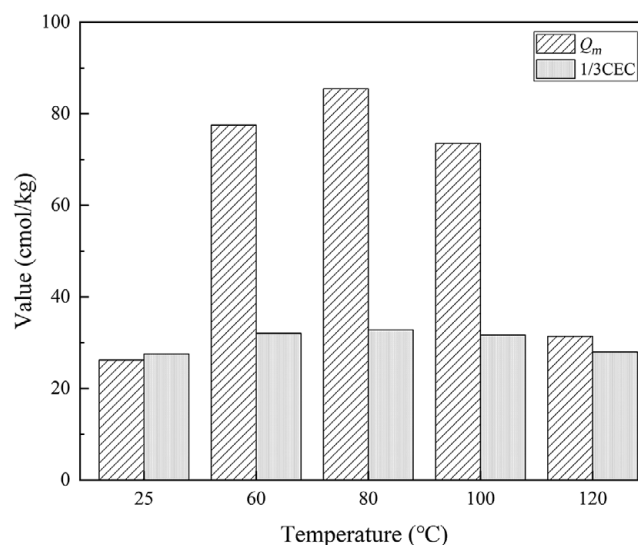

Figure 7. Comparison between the maximum adsorption capacity of Eu^{3+} and 1/3 CEC.

This indicates that the adsorption capacity of Eu^{3+} on these two minerals was predominantly driven by cation exchange. However, the transition state samples at temperatures ranging from 60 to 100°C mainly exhibit complex adsorption. This phenomenon shows that a large number of hydroxyl groups was generated during the smectite lattice fragmentation process, leading to an increase in complex adsorption with Eu^{3+}. On the contrary, during the transformation from albite to analcime, the bonding of tetrahedral groups leads to a decrease in hydroxyl groups, resulting in a reduction in the complex adsorption of Eu^{3+}. Therefore, the adsorption evolution of smectite on nuclide Eu^{3+} was mainly caused by the increase and decrease of the hydroxyl group, which is also the result of crystal dissociation and tetrahedral structure reconstruction.

Conclusions

Based on the analysis and study of mineral composition, micromorphology, SSA, pore structure, CEC, and Eu^{3+} adsorption capacity of dissolved bentonites at different temperatures under hyperalkaline conditions, the following conclusions can be drawn:

(1) Temperature significantly impacts mineral stability in hyperalkaline solution. The alkali dissolution rate of fine-grained cristobalite in bentonite exceeds that of smectite. At 60°C, in a NaOH solution with pH=14, the aluminum-oxygen octahedron within the layered smectite crystal structure collapses; at 80°C, the crystal lattices break completely, and the Al/SiO_4 tetrahedral units reassemble into a loose framework structure resembling albite; at 100°C, this loose framework transforms into a more stable and dense framework structure characteristic of analcime.

(2) During the phase transition of smectite into albite, the SSA of the mineral reduces significantly, layer fracture pores disappear gradually, a large number of polar negative sites will be exposed to increase the CEC, and a large number of hydroxyl groups are generated to increase the complex adsorption amount of Eu^{3+}. During the transformation of albite into analcime, the lamellar mineral aggregate consolidates and reconstructs to form tetrakisoctahedron crystalline particles. The SSA of the mineral changes a little, the pores become columnar through pores, and the polar negative sites are wrapped in the zeolite particles, resulting in the reduction of CEC. Simultaneously, a large number of hydroxyl groups condense and are consumed, reducing the amount of complex adsorption with Eu^{3+}.

(3) The active hydroxyl site of the smectite surface exists not only at the edge but also at the position where isomorphous substitution occurs. In the process of dissolution, the smectite lamellar assemblages develop from holes to sharp-edged assemblage fragments, then consolidate into plates, and finally become tetrakisoctahedron particles. The SSA reduces significantly by the transition from a layered structure to a frame structure.

This experiment for evolutionary bentonite behavior in NaOH solution has limitations as it is uncertain whether other ions would form other minerals. However, one certainty is that the layered structure of the smectite crystal breaks down and reconstitutes into frame-like structure minerals in hyperalkaline conditions. Specifically, smectite first transforms into feldspar-group minerals and then into zeolite-group minerals. The bentonite-mineral adsorption performance increases at temperatures of <80°C and then decreases sharply. This observation is useful for designing the operating temperature of the repository.

Author contributions. Rao-ping Liao: Investigation, Formal analysis, Writing-Original draft preparation; **Yong-gui Chen:** Conceptualization, Supervision, Funding acquisition; **Chuang Yu:** Supervision, Resources; **Wei-min Ye:** Conceptualization; **Dong-bei Wu:** Writing- review and editing; **Cong Liu:** Writing-review and editing; Qiong Wang: Writing- review and editing.

References

Al-Ghouti, M.A., & Da'ana, D.A. (2020) Guidelines for the use and interpretation of adsorption isotherm models: A review. *Journal of Hazardous Materials*, *393*, 122383. https://doi.org/10.1016/j.jhazmat.2020.122383

Anh, H.N., Ahn, H., Jo, H.Y., & Kim, G.-Y. (2017). Effect of alkaline solutions on bentonite properties. *Environmental Earth Sciences*, *76*(10), 374. https://doi.org/10.1007/s12665-017-6704-8

Chen, Y.-G., Liu, L.-N., Ye, W.-M., Cui, Y.-J., & Wu, D.-B. (2019). Deterioration of swelling pressure of compacted Gaomiaozi bentonite induced by heat combined with hyperalkaline conditions. *Soils and Foundations*, *59*(6), 2254–2264. https://doi.org/10.1016/j.sandf.2019.12.008

Cheshire, M.C., Caporuscio, F.A., Rearick, M.S., Jové-Colón, C., & McCarney, M.K. (2014). Bentonite evolution at elevated pressures and temperatures: An experimental study for generic nuclear repository designs. *American Mineralogist*, *99*(8–9), 1662–1675. https://doi.org/10.2138/am.2014.4673

Cuevas, J., Cabrera, M.Á., Fernández, C., Mota-Heredia, C., Fernández, R., Torres, E., Turrero, M.J., & Ruiz, A.I. (2022). Bentonite Powder XRD Quantitative Analysis Using Rietveld Refinement: Revisiting and Updating Bulk Semiquantitative Mineralogical Compositions. *Minerals*, *12*(6), Article 6. https://doi.org/10.3390/min12060772

Fernández, R., Cuevas, J., Sánchez, L., de la Villa, R. V., & Leguey, S. (2006). Reactivity of the cement–bentonite interface with alkaline solutions using transport cells. *Applied Geochemistry*, *21*(6), 977–992. https://doi.org/10.1016/j.apgeochem.2006.02.016

Fernández, A.M., & Villar, M.V. (2010). Geochemical behaviour of a bentonite barrier in the laboratory after up to 8 years of heating and hydration. *Applied Geochemistry*, *25*(6), 809–824. https://doi.org/10.1016/j.apgeochem.2010.03.001

Freundlich, H. (1907) Über die adsorption in lösungen. *Zeitschrift Für Physikalische Chemie*, *57U*(1), 385–470. https://doi.org/10.1515/zpch-1907-5723

García-Romero, E., Lorenzo, A., García-Vicente, A., Morales, J., García-Rivas, J., & Suárez, M. (2021) On the structural formula of smectites: A review and new data on the influence of exchangeable cations. *Journal of Applied Crystallography*, *54*(1), 251–262. https://doi.org/10.1107/S1600576720016040

Gens, A., Vasconcelos, R.B. de, & Olivella, S. (2020) Towards higher temperatures in nuclear waste repositories. *E3S Web of Conferences*, *205*, 01001. https://doi.org/10.1051/e3sconf/202020501001

González-Santamaría, D.E., Justel, A., Fernández, R., Ruiz, A.I., Stavropoulou, A., Rodríguez-Blanco, J.D., & Cuevas, J. (2021) SEM-EDX study of bentonite alteration under the influence of cement alkaline solutions. *Applied Clay Science*, 212, 106223. https://doi.org/10.1016/j.clay.2021.106223

Grybos, M., Michot, L.J., Skiba, M., Billard, P., & Mustin, C. (2010) Dissolution of anisotropic colloidal mineral particles: Evidence for basal surface reactivity of nontronite. *Journal of Colloid and Interface Science*, 343(2), 433–438. https://doi.org/10.1016/j.jcis.2009.11.058

Kale, R.C., Kapil, B., & Ravi, K. (2021) Response of compacted bentonite to hyperalkalinity and thermal history. *Scientific Reports*, 11(1), 15483. https://doi.org/10.1038/s41598-021-95023-5

Karnland, O., Olsson, S., Nilsson, U., & Sellin, P. (2007) Experimentally determined swelling pressures and geochemical interactions of compacted Wyoming bentonite with highly alkaline solutions. *Physics and Chemistry of the Earth, Parts A/B/C*, 32(1–7), 275–286. https://doi.org/10.1016/j.pce.2006.01.012

Kurniawan, T.A., Othman, M.H.D., Singh, D., Avtar, R., Hwang, G.H., Setiadi, T., & Lo, W. (2022) Technological solutions for long-term storage of partially used nuclear waste: A critical review. *Annals of Nuclear Energy*, 166, 108736. https://doi.org/10.1016/j.anucene.2021.108736

Kuwahara, Y. (2006) In-situ AFM study of smectite dissolution under alkaline conditions at room temperature. *American Mineralogist*, 91(7), 1142–1149. https://doi.org/10.2138/am.2006.2078

Kyzioł-Komosińska, J., Janeczek, J., Krzykawski, T., Fabiańska, M. J., Matuszewska, A., Dzieniszewska, A., Teper, E., Pająk, M., & Sawicka, N. (2019) Adsorption of Eu(III) onto bentonite and phyllite: A comparative study. *Applied Clay Science*, 183, 105330. https://doi.org/10.1016/j.clay.2019.105330

Langmuir, I. (1918) The adsorption of gases on plane surfaces of glass, mica and platinum. *Journal of the American Chemical Society*, 40(9), 1361–1403. https://doi.org/10.1021/ja02242a004

Lee, J.H., Kim, J., Kwon, J.-S., & Jo, H.Y. (2023) Effect of hydrothermal alteration of Ca-bentonite in K-rich solutions with different pHs on the physicochemical, swelling, and Cs adsorption properties. *Applied Geochemistry*, 158, 105791. https://doi.org/10.1016/j.apgeochem.2023.105791

Liao, R., Yu, C., Chen, Y., Ye, W., Chen, Z., Wu, D., Zeng, Z., & Wang, Q. (2023) Preparation and characterization of carboxylic polymer grafted GMZ bentonite for the adsorption of Eu^{3+} nuclide. *Environmental Earth Sciences*, 82(5), 129. https://doi.org/10.1007/s12665-023-10828-z

Liu, J., Tang, W., Li, J., Zhang, J., Guo, Z., Chen, L., & Liu, Y. (2021) An experimental research on swelling pressure of GMZ Na-bentonite submitted to the strong alkali-heat environment. *Rock and Soil Mechanics*, 42(8), 2160–2184. https://doi.org/10.16285/j.rsm.2020.1779

Liu, L.-N., Chen, Y.-G., Ye, W.-M., Cui, Y.-J., & Wu, D.-B. (2018) Effects of hyperalkaline solutions on the swelling pressure of compacted Gaomiaozi (GMZ) bentonite from the viewpoint of Na^+ cations and OH– anions. *Applied Clay Science*, 161, 334–342. https://doi.org/10.1016/j.clay.2018.04.023

Liu, L.-N., Chen, Y.-G., Ye, W.-M., Cui, Y.-J., & Wu, D.-B. (2022) Swelling pressure deterioration of compacted GMZ bentonite and its structural damage under heat combined with hyperalkaline conditions. *Geomechanics and Geoengineering*, 17(1), 297–308. https://doi.org/10.1080/17486025.2020.1739755

Liu, Z.-R., Ye, W.-M., Zhu, J.-C., Chen, Y.-G., & Wang, Q. (2023) Temperature and alkaline solution effects on the hydro-mechanical behaviours of GMZ bentonite pellet mixtures. *Acta Geotechnica*, 18(11), 6097–6110. https://doi.org/10.1007/s11440-023-02044-7

Nightingale, E.R. (1959) Phenomenological theory of ion solvation. Effective radii of hydrated ions. *The Journal of Physical Chemistry*, 63(9), 1381–1387. https://doi.org/10.1021/j150579a011

Ramírez, S., Cuevas, J., Vigil, R., & Leguey, S. (2002) Hydrothermal alteration of "La Serrata" bentonite (Almeria, Spain) by alkaline solutions. *Applied Clay Science*, 21(5), 257–269. https://doi.org/10.1016/S0169-1317(02)00087-X

Refson, K., Park, S.-H., & Sposito, G. (2003) Ab initio computational crystallography of 2:1 clay minerals: 1. Pyrophyllite-1Tc. *The Journal of Physical Chemistry B*, 107(48), 13376–13383. https://doi.org/10.1021/jp0347670

Rozalen, M., Huertas, F. J., & Brady, P. V. (2009) Experimental study of the effect of pH and temperature on the kinetics of montmorillonite dissolution.

Geochimica et Cosmochimica Acta, 73(13), 3752–3766. https://doi.org/10.1016/j.gca.2009.03.026

Samper, J., Mon, A., & Montenegro, L. (2020) A coupled THMC model of the geochemical interactions of concrete and bentonite after 13 years of FEBEX plug operation. *Applied Geochemistry*, 121, 104687. https://doi.org/10.1016/j.apgeochem.2020.104687

Sposito, G., Skipper, N.T., Sutton, R., Park, S., Soper, A.K., & Greathouse, J.A. (1999) Surface geochemistry of the clay minerals. *Proceedings of the National Academy of Sciences of the United States of America*, 96(7), 3358–3364. https://www.jstor.org/stable/47645

Sun, Z., Chen, Y., & Ye, W. (2022) A systematic review of bentonite/concrete interaction system in HLW disposal repositories: Theoretical, experimental and geochemical modelling analysis. *Construction and Building Materials*, 353, 129075. https://doi.org/10.1016/j.conbuildmat.2022.129075

Tong, Y., Zhang, H., Zhou, G., & Li, X. (2022) Mineralogical evidence of alkaline corrosion of montmorillonite in GMZ bentonite. *Rock and Soil Mechanics*, 43(11), 2973–2982. https://doi.org/10.16285/j.rsm.2021.2174

Tyupina, E. A., Kozlov, P. P., & Krupskaya, V. V. (2023) Application of cement-based materials as a component of an engineered barrier system at geological disposal facilities for radioactive waste – A review. *Energies*, 16(2), Article 2. https://doi.org/10.3390/en16020605

Wang, J., & Guo, X. (2020) Adsorption isotherm models: Classification, physical meaning, application and solving method. *Chemosphere*, 258, 127279. https://doi.org/10.1016/j.chemosphere.2020.127279

Wang, J., Chen, L., Su, R., & Zhao, X. (2018) The Beishan underground research laboratory for geological disposal of high-level radioactive waste in China: Planning, site selection, site characterization and in situ tests. *Journal of Rock Mechanics and Geotechnical Engineering*, 10(3), 411–435. https://doi.org/10.1016/j.jrmge.2018.03.002

Wang, J., Wang, J., Zeng, F., & Wu, X. (2011) Molecular simulations of crystal structure conformation, X-Ray diffraction and infra-red spectrum in montmorillonites (in Chinese). *Acta Mineralogical Sinica*, 31(1) https://link.cnki.net/doi/10.16461/j.cnki.1000-4734.2011.01.020

Wang, X., Sun, Y., Alsaedi, A., Hayat, T., & Wang, X. (2015) Interaction mechanism of Eu(III) with MX-80 bentonite studied by batch, TRLFS and kinetic desorption techniques. *Chemical Engineering Journal*, 264, 570–576. https://doi.org/10.1016/j.cej.2014.11.136

Xu, T., Senger, R., & Finsterle, S. (2011) Bentonite alteration due to thermal-hydro-chemical processes during the early thermal period in a nuclear waste repository. *Nuclear Technology*, 174(3), 438–451. https://doi.org/10.13182/NT11-A11751

Ye, W.M., Zheng, Z.J., Chen, B., Chen, Y.G., Cui, Y.J., & Wang, J. (2014) Effects of pH and temperature on the swelling pressure and hydraulic conductivity of compacted GMZ01 bentonite. *Applied Clay Science*, 101, 192–198. https://doi.org/10.1016/j.clay.2014.08.002

Ye, W.-M., Chen, Y.-G., Chen, B., Wang, Q., & Wang, J. (2010) Advances on the knowledge of the buffer/backfill properties of heavily-compacted GMZ bentonite. *Engineering Geology*, 116(1), 12–20. https://doi.org/10.1016/j.enggeo.2010.06.002

Ye, W.M., He, Y., Chen, Y.G., Chen, B., & Cui, Y. J. (2016). Thermochemical effects on the smectite alteration of GMZ bentonite for deep geological repository. *Environmental Earth Sciences*, 75(10), 906. https://doi.org/10.1007/s12665-016-5716-0

Yokoyama, S., Shimbashi, M., Minato, D., Watanabe, Y., Jenni, A., & Mäder, U. (2021a) Alteration of bentonite reacted with cementitious materials for 5 and 10 years in the Mont Terri Rock Laboratory (CI Experiment). *Minerals*, 11(3), Article 3. https://doi.org/10.3390/min11030251

Yokoyama, S., Shimbashi, M., Minato, D., Watanabe, Y., Jenni, A., & Mäder, U. (2021b) Alteration of Bentonite Reacted with Cementitious Materials for 5 and 10 years in the Mont Terri Rock Laboratory (CI Experiment). *Minerals*, 11(3), Article 3. https://doi.org/10.3390/min11030251

Zhang, H., Tong, Y., & Jia, Q. (2020) Corrosion of GMZ bentonite by diffusion of strong alkaline solution (in Chinese) *Chinese Journal of Rock Mechanics and Engineering*, 39(1), 166–176. https://doi.org/10.13722/j.cnki.jrme.2019.0417

Zhu, J., Wang, T., Zhang, H., & Zhou, G. (2023) Alkaline buffer characteristics and mechanism of Gaomiaozi bentonite in high-level radioactive waste repository. *Environmental Earth Sciences*, 82(13), 346. https://doi.org/10.1007/s12665-023-10928-w